

# Physicochemical properties and storage stability of nanoencapsulated docosahexaenoic acid with different gum arabic Maillard reaction products

L. Zhou<sup>a</sup>, S. Yuan<sup>a</sup>, T. Chang<sup>a</sup>, T. Li<sup>a</sup>, J. Hao<sup>a</sup> and J. Liu<sup>a</sup>

<sup>a</sup> College of Food and Biology, Hebei University of Science and Technology, Shijiazhuang, 050000, China

<sup>✉</sup> Corresponding author: 1308676013@qq.com

Submitted: 17 October 2024; Accepted: 16 January 2025; Published: 15 April 2025.

**SUMMARY:** In this study, the polysaccharide gum arabic (GA) and proteins, including sodium caseinate (SC), soy protein isolate (SPI), and gelatin (GE) Maillard reaction products (MRPs), were used as encapsulating materials for making docosahexaenoic acid (DHA) nanoemulsions. The optimum conditions were as follows: ultrasonic power 585 W, ultrasonic time 20 min, total mass concentration 5%, core wall ratio 1:2. Scanning electron microscope, transmission electron microscopy, and Fourier transform infrared analysis confirmed the effective encapsulation of DHA oil by the SC/GA, SPI/GA, and GE/GA MRPs, providing core protection. The thermogravimetric analysis shows that SPI/GA MRPs-DHA nanoparticles have good thermal stability. Additionally, SPI/GA MRPs-DHA nanoparticles exhibited the lowest moisture content (1.53%) and wetting time (183 s) and the highest solubility (97.05%), encapsulation efficiency (89.57%), and loading capacity (44.79%), with good oxidative and emulsion stability. This indicates that SPI/GA MRPs may be a better wall material for nanoencapsulated DHA.

**KEYWORDS:** DHA; Gum arabic; Maillard reaction products; Nanoemulsion; Nanoparticle; Sodium caseinate; Storage stability; Soy protein isolate.

**RESUMEN:** *Propiedades fisicoquímicas y estabilidad de almacenamiento del ácido docosahexaenoico nanoencapsulado con diferentes productos de Maillard de goma arábica.* En este estudio, se utilizaron los productos de la reacción de Maillard (MRPs) de la goma arábica (GA), un polisacárido, y las proteínas, incluyendo el caseinato de sodio (SC), el aislado de proteína de soja (SPI) y la gelatina (GE), como materiales encapsulantes para la fabricación de nanoemulsiones de ácido docosahexaenoico (DHA). Las condiciones óptimas fueron las siguientes: potencia de ultrasonido 585 W, tiempo ultrasonido 20 min, concentración de masa total 5%, relación de la pared del núcleo 1:2. El microscopio electrónico de barrido, la microscopía electrónica de transmisión y el análisis infrarrojo por transformada de Fourier confirmaron la encapsulación efectiva del aceite de DHA por los MRPs SC/GA, SPI/GA y GE/GA, proporcionando protección del núcleo. El análisis termogravimétrico muestra que las nanopartículas de MRPs-DHA SPI/GA tienen una buena estabilidad térmica. Además, las nanopartículas de MRPs-DHA de SPI/GA mostraron el menor contenido de humedad (1,53%) y tiempo de humectación (183 s) y la mayor solubilidad (97,05%), eficiencia de encapsulación (89,57%) y capacidad de carga (44,79%), con buenas estabilidades oxidativa y de emulsión. Esto indica que los MRPs de SPI/GA pueden ser los mejores materiales de pared para el DHA nanoencapsulado.

**PALABRAS CLAVE:** Aislado de proteína de soja; Caseinato de sodio; DHA; Estabilidad en almacenamiento; Goma arábica; Nanoemulsión; Nanopartícula; Productos de la reacción de Maillard.

**Citation/Cómo citar este artículo:** Zhou L, Yuan S, Chang T, Li T, Hao J, Liu J. 2024. Physicochemical properties and storage stability of nanoencapsulated docosahexaenoic acid with different gum arabic Maillard reaction products. *Grasas Aceites* 75 (4), 2254. <https://doi.org/10.3989/gya.1094241.2254>.

**Copyright:** ©2024 CSIC. This is an open-access article distributed under the terms of the Creative Commons Attribution 4.0 International (CC BY 4.0) License.

## 1. INTRODUCTION

DHA is the most important omega-3 fatty acid, and there is a growing demand for DHA because of its many health benefits related to cholesterol, cardiovascular disease, inflammation, early childhood

development, and psychiatric disorders. However, since DHA presents low aqueous solubility and a fishy odor, it is unsuitable for direct consumption. In addition, the presence of unsaturated bonds in DHA makes it highly susceptible to oxidation, leading to the development of rancid odor and taste, as well as a

subsequent reduction in its health-promoting effects (Lv and Xu, 2022). In this context, nanoencapsulation technology offers a novel strategy to overcome these limitations.

In recent years, nanotechnology has received more and more attention from the food sector due to both the minimum particle size and a significant surface area, giving nanostructured materials their exceptional properties and capabilities for their application in the food industry (Awuchi *et al.*, 2022). The most appropriate nanoscale carrier materials for food applications are carbohydrate, protein, or lipid-based alternatives. When preparing oil-in-water emulsions, those stabilized exclusively by proteins often exhibit insufficient stability. In contrast, polysaccharides have been shown to effectively stabilize emulsions under a range of environmental conditions. Consequently, the incorporation of polysaccharides into protein-stabilized emulsions can significantly enhance their stability. At the same time, the interaction between protein and polysaccharide improves the solubility, colloid stability and interface function of protein (Anal *et al.*, 2019). Therefore, polysaccharide - protein nanostructures are more beneficial than pure single biopolymer nanoparticles (NPs). In a current study, whey proteins and pectin were used to nanoencapsulate D-limonene, and the results suggested that these wall materials would be able to nanoencapsulate (encapsulation efficiency of 88%) D-limonene at high stability (83.0–98.5%) (Ghasemi *et al.*, 2018). Ghasemi *et al.*, (2017) studied the encapsulation of orange peel oil by pectin-whey-protein nanocomplexes, and the nanocomplexes can improve the stability of orange peel oil.

GA is abundantly applied for nanoencapsulation, owing to its desirable solubility, low viscosity, emulsifying properties, and the high holding capacity of oil droplets (Moghadam *et al.*, 2019). Proteins (SC, SPI, and GE) also have significant dietary value and abundant functional properties, for example, gelation, emulsification, or water binding capacity. Furthermore, the use of SC/GA MRPs, SPI/GA MRPs and GE/GA MRPs as wall materials for the nanoencapsulation of DHA has received limited attention in the literature. Protein-carbohydrate MRPs show superior emulsification, strong antioxidative activity, and good pH stability, so they are considered to be good wall materials for novel encapsulation systems for unsaturated oils. A high EE of DHA (93.88,

94.4, and 78.88%) can be found in the literature (Liu *et al.*, 2023; Botrel *et al.*, 2014; Ilyasoglu and El, 2014). However, the LC has been less reported than the EE. The DHA oil LC is considered relatively low at 11.9% (Liu *et al.*, 2023), 31.46% (Botrel *et al.*, 2014), and 32.66% (Ilyasoglu and El, 2014). A high EE at a high LC is much more attractive and important for producers and has rarely been reported in the literature, which also offers numerous advantages, such as minimizing wall material, reducing product volume and weight, and effectively controlling the product's antioxidant properties.

In this paper, SC/GA MRPs, SPI/GA MRPs and GE/GA MRPs were chosen as wall materials for the preparation of DHA nanoencapsulated materials. The optimal preparation conditions were determined by systematically varying the total mass concentration, ultrasonic time, and core-wall ratio of the composite system. The DHA NPs were comprehensively characterized utilizing multiple analytical techniques, including OM, SEM, TEM, TGA, and FTIR. Furthermore, both their physical and chemical properties, encapsulation efficiency, and loading capacity were quantified, and their emulsification and oxidation stability were assessed. These assessments were conducted to determine the best MRP that can provide effective protection for DHA and the best preparation process for DHA nanocapsules. It provides ideas for the application and storage of DHA in the food industry.

## 2. MATERIALS AND METHODS

### 2.1. Materials

DHA, a light-yellow oily liquid extracted from algae, was obtained from Hubei Fuxing Biotechnology Co., Ltd. (Hubei, China). Gum Arabic (dry matter content of 85%) was purchased from Taian Dingli Gum Industry Co., Ltd. (Shangdong, China). Sodium caseinate (protein content of 88%) was obtained from Roe Reagent Co., Ltd. Soy protein isolate (protein content of 90%) was purchased from Jiangsu Fushengde Bioengineering Co., Ltd. (Jiangsu, China). Gelatin (protein content of 85%) was purchased from Rousselot Gelatin Co., Ltd (Guangdong, China). Modified soybean lecithin was supplied by Chinaholder Biotech Co., Ltd (Beijing, China). Other chemicals used were of analytical grade.

## 2.2. Preparation of MRPs

The approach reported by Pirestani *et al.* (2018) was used with modifications. SC, SPI, GE, and GA were mixed in distilled water for dispersion, during which the concentrations of SC, SPI, GE, and GA were 1 (w/v) and 2% (w/v), respectively. The mixture of the two biopolymers was stirred with a magnetic stirrer for 2 h at room temperature. The pH of the dispersion was adjusted to 7.5 by carefully adding 0.1 M NaOH, followed by gently stirring overnight at 4 °C to completely hydrate the biopolymer mixture. The solution of the two biopolymers was heated at 85 °C for 90 min and then immediately cooled in an ice-water bath to stop the reaction. The resulting product was freeze-dried and stored for later use.

### 2.2.1. Optimization of the MRPs-DHA NMs preparation process

The approach as reported by Li *et al.* (2022) was used with modifications. A certain amount of wall material was weighed and stirred into deionized water until it was completely dissolved. Subsequently, a specific quantity of DHA was weighed and added to the solution, which was then stirred for 30 minutes to form the composite system solution. Then a high-speed shear machine was used to shear for 3 min at a speed of 12000r/min, and then an ultrasonic homogenizing was kept for 20 minutes at an ultrasonic power of 585w to obtain the MRPs-DHA NMs. A single-factor strategy was used to investigate the influence of three independent variables (total mass concentration of composite system, ultrasonic time, and core-wall ratio) on the preparation of MRPs-DHA NMs. Particle size and PDI are taken as the assessment indices of encapsulation. The total mass concentration of the composite system was 1, 5, 10, 15, and 20%. The ultrasonic time was 20, 15, 20, 25, and 30 mins, while core-wall ratio was 1:1, 1:2, 1:3, 1:4, and 1:5 w/w, respectively.

The prepared solution was pre-frozen at -20 °C in advance and then dried in a freeze dryer for approximately 48 h. The obtained MRPs-DHA NPs were sealed and stored in a freezer at -20 °C.

### 2.2.2. Freeze drying

The obtained SC/GA MRPs-DHA NMs, SPI/GA MRPs-DHA NMs and GE/GA MRPs-DHA NMs

were poured into Petri dishes and stored at -18 °C overnight. Frozen NMs were dried in a laboratory-scale freeze-drier (Biocool limited-FD-1A-50, China) to obtain SC/GA MRPs-DHA NPs, SPI/GA MRPs-DHA NPs and GE/GA MRPs-DHA NPs. The freeze-drying process was performed at a temperature of -50 °C and a vacuum pressure of 20 Pa, with a duration of 48 hours. The final powder was stored at 4 °C until use.

## 2.3. Analytical determinations

### 2.3.1. Particle size and polydispersity index (PDI) measurement

The three freshly prepared NMs were sealed and stored for 30 days (at 25 °C). The samples were taken every 5 days to determine the particle size and PDI. Average particle size and PDI of DHA emulsions were measured by dynamic light scattering (Zetasizer Nano SZ-100, Horiba, Japan) technique at 25 °C. Three replicate measurements were performed for each sample.

### 2.3.2. CI measurement (Hosseini *et al.*, 2015)

The creaming of emulsion samples (10 mL) was monitored at room temperature by visual observation of the height of the serum layer formed at the bottom of glass tubes (*HS*), expressed as a percentage of the total height of the emulsions in the tubes (*HE*):

$$CI(\%) = \frac{HS}{HE} \times 100\% \quad (1)$$

### 2.3.3. Determination of moisture content

Exactly 1 g of the samples was dried at 105 °C until a constant mass was achieved. The moisture content was calculated using the following formula:

$$\text{Moisture content}(\%) = \frac{m - m_1}{m} \times 100\% \quad (2)$$

Where *m* is the mass of the sample/g, and *m*<sub>1</sub> is the mass of the sample after drying.

### 2.3.4. Determination of solubility

Exactly 1 g of the powder sample was weighed into a 50 mL beaker and dissolved in a 50 mL cen-

trifuge tube with 30 mL of water at 25-30 °C. The centrifuge tube was placed in water at 30 °C for heat preservation for 5 min, and then taken out and shaken for 3 min. The tube was centrifuged for 10 min at 3000 rpm and the supernatant was removed. Then, 30 mL of water at 25-30 °C were added to the centrifuge tube, which was sealed with a plug. Shaking and centrifugation were carried out again under the same conditions. After centrifugation twice, the sediment was transferred to a weighing dish and dried at 105 °C until a constant weight (the last two mass differences did not exceed 2 mg). The solubility of the samples was calculated according to the following formula:

$$X(\text{g}/100\text{ g}) = 100 - \frac{(m_1 - m_2) \times 100}{m_3} \quad (3)$$

Where X is the solubility and  $m_1$  is the mass of the weighing dish and the insoluble matter.  $m_2$  and  $m_3$  are the mass of the weighing dish and the sample, respectively.

### 2.3.5. Determination of wettability

Approximately 0.1 g of the powder sample was dispersed in 100 mL of deionized water and allowed to wet naturally without stirring. The time taken for the last powder particle of each sample to be completely soaked with water was recorded to assess wettability. Each group was measured three times.

### 2.3.6. EE and LC measurement

The amount of surface oil was determined according to the method of petroleum ether extraction (García *et al.*, 2005) and conducted according to the study by Botrel *et al.* (2014). In this study, the total oil content was calculated as the initial amount of oil added because algal oil is nonvolatile. In addition, the degradation of oil at high temperatures attached to the dryer wall is considered to be negligible (Jafari *et al.*, 2008). The EE and LC were calculated using the following equations:

$$\text{EE}(\%) = \frac{\text{Total oil-surface oil}}{\text{Total oil}} \times 100\% \quad (4)$$

$$\text{LC}(\%) = \frac{m_0 - m_1}{M} \times 100\% \quad (5)$$

Where  $M$  is the mass of the MRPs wall material quality,  $m_0$  is the mass of the initially added DHA, and  $m_1$  is the mass of the unembedded DHA.

### 2.3.7. OM analysis

10  $\mu\text{L}$  of emulsion sample were smeared over a grease-free glass slide and visualized under a light microscope (Dey *et al.*, 2019).

### 2.3.8. SEM analysis

A Shimadzu S4800 apparatus was used to view the surface morphology of NPs by SEM analysis. The sample was attached to a two-sided adhesive tape and mounted on stubs, and redundant powder samples were removed. The NPs were then sprayed with gold, and investigated under SEM, which was operated at an acceleration voltage of 5 kV (Su *et al.*, 2021).

### 2.3.9. TEM analysis

The morphologies and sizes of the NMs were recorded using a TEM (HT7700, Hitachi, Japan) operating at an acceleration voltage of 80 kV. A tiny drop of the NM (20  $\mu\text{L}$ ) was deposited onto a carbon-coated copper grid, and excess water was blotted with filter paper (Su *et al.*, 2021).

### 2.3.10. TGA

TGA2 Mettler Toledo, Zurich, Switzerland was employed to evaluate the thermal behavior of dried nanocapsules. DHA, MRPs wall materials, and DHA-loaded NPs products were placed in an aluminum specimen box at a heating rate of 10 °C/min from 50 to 500 °C under nitrogen injection as a pure gas with a flow rate of 20 mL/min and a sample weight of 5 mg (Wang *et al.*, 2020). During the heating process, TG/Derivative thermogravimetry (DTG) curves were carried out.

### 2.3.11. FTIR analysis

The FTIR spectroscopy of DHA, MRPs wall materials, and DHA-loaded NPs products was carried out using a Nicolet iS10 FTIR spectrometer, with a resolution of 2  $\text{cm}^{-1}$  in 64 scans. A thin plate of potassium bromide was used as the background.

Briefly, a 2.0 mg freeze-dried sample was mixed with 198 mg pure potassium bromide (KBr) powder. The mixture was pressed into pellets and measured by FTIR at 500-4000  $\text{cm}^{-1}$  (Liu *et al.*, 2021).

### 2.3.12. Accelerated storage test

The oxidative stability of the MRPs-DHA NPs was assessed using the Schaal oven test, where dry powder samples were added to glass bottles and kept in an oven at  $60 \pm 1$  °C for 72 hours for accelerated oxidation. The POV was determined in accordance with the standard of the People's Republic of China (GB/T 5009.37-2003). The sample was weighed and dissolved in a mixture of chloroform and methanol ( $v/v = 7:3$ ) to make a 10 mL solution, which is referred to as sample solution 1 in the following text. 1.0 mL of sample solution 1 was pipetted into a test tube, to which 1 drop of ferrous chloride solution (3.5 g/L) was added, followed by dilution to 10 mL with the chloroform-methanol mixture. This diluted solution is referred to as sample solution 2. After adding 1 drop of potassium thiocyanate solution (300 g/L), the mixture was left at 20°C for 5 minutes. The absorbance was measured at a wavelength of 500 nm, using a mixture of chloroform and methanol ( $v/v = 7:3$ ) as the blank. The concentration of ferrous ions in sample solution 2 was obtained using a calibration curve. The POV in the sample was calculated using the following formula.

$$\text{POV (meq/kg)} = \frac{c - c_0}{m \times \frac{V_2}{V_1} \times 55.84 \times 2} \quad (6)$$

Where,  $c$  is the equivalent of iron concentration ( $\mu\text{g/mL}$ ) in the sample solution 2;  $c_0$  is the equivalent of iron concentration ( $\mu\text{g/mL}$ ) in the reference containing 1 drop of ferrous-chloride, 1 drop of potassium-thiocyanate, and chloroform-methanol mixture;  $V_2/V_1 = 10$ , which is the dilution ratio during the preparation of sample solution 2;  $m$  is the sample mass, the unit is g.

### 2.4. Statistical analysis

All experiments were performed in triplicate and the mean values were recorded. All data were analyzed using SPSS statistical software. Analysis of variance (ANOVA) and means with significant dif-

ferences ( $p < 0.05$ ) were determined using the Fisher least significant difference (LSD) test.

## 3. RESULTS

### 3.1. Effect of process factors on MRPs-DHA NM preparation

The effects of the total mass concentration of the composite system on the particle size and PDI of the DHA NMs are shown in Figure 1 (A, D). For the GE/GA MRPs-DHA NMs, particle size larger than 1000 nm is considered nonsensical. These particles are unstable and tend to precipitate or form a cream during storage, and the corresponding data are not shown in Figure 1 (A, D). As depicted in Figure 1 (A, D), the particle size of the SC/GA MRPs-DHA NMs, SPI/GA MRPs-DHA NMs and GE/GA MRPs-DHA NMs increased with increasing total mass concentration of the composite system. This increase is likely due to a higher concentration of both the core and wall materials, as well as a greater number of complex and emulsion droplets, which raised the likelihood of collision and aggregate formation.

A low PDI indicates a limited size distribution, which indicates excellent stability and homogeneity of the NMs. For the SPI/GA MRPs-DHA NMs, the PDI increased with the increasing total mass concentration of the composite system. SC/GA MRPs-DHA NMs showed the lowest PDI value at a 5% total mass concentration of the composite system, and the PDI of GE/GA MRPs-DHA NMs tended to initially increase, then decrease and increase again. International standard organizations (ISOs) state that PDI values above 0.7 indicate a wider size distribution while values below 0.05 are linked to monodisperse samples (Mudalige *et al.*, 2019). The PDI values for SC/GA MRPs-DHA NMs, SPI/GA MRPs-DHA NMs and GE/GA MRPs-DHA NMs are nearly all below 0.5, which denotes strong stability. Consequently, to achieve a more stable and uniform system with a greater wall material concentration and loading capacity, an ideal total mass concentration of 5% for the composite system was selected in this work.

The effects of ultrasonic time on the particle size and PDI of the DHA NMs are shown in Figure 1 (B, E). For the GE/GA MRPs-DHA NMs, particle size data larger than 1000 nm are not shown in Figure 1 (B, E). Based on the data presented in Figure 1 (B, E),

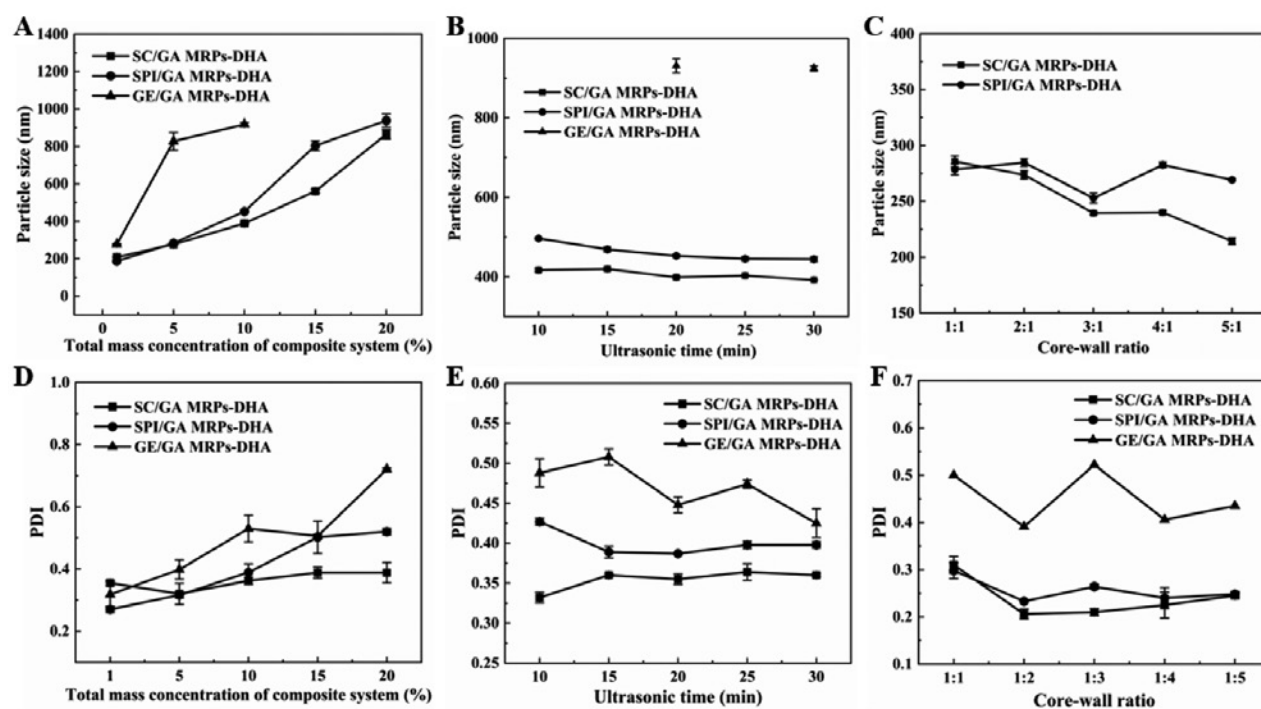


FIGURE 1. Effect of process factors on MRP-DHA NM preparation. Total mass concentration of composite system (A, D; sample ultrasonic time 20 minutes, core-wall ratio 1:3). Ultrasonic time (B, E; total mass concentration of sample composite system 10%, core-wall ratio 1:3). Core-wall ratio (C, F; total mass concentration of sample composite system 10%, ultrasonic time 20 minutes). The results are expressed as mean  $\pm$  standard deviation ( $n = 3$ ).

the particle sizes of the SC and SPI/GA MRP-DHA NMs decreased as the ultrasonic time increased, reaching a minimum at a specific point when the ultrasonic power was set to 585 W. It is important to observe that beyond a certain point, further increasing the processing time does not lead to a significant reduction in particle size. As a result, to obtain the smallest particle size, it is unnecessary to prolong the ultrasonic time beyond a specific threshold. Additionally, the PDI of SC/GA MRP-DHA NMs and SPI/GA MRP-DHA NMs remained steady when the ultrasonic time exceeded 15 minutes. The total PDI of GE/GA MRP-DHA NMs decreased with increasing ultrasonic time. It is recommended that an ultrasonic time of 20 minutes is adequate to attain the intended particle size reduction, considering both particle size and PDI.

The effects of core-wall ratio on the particle size and PDI of the DHA NMs are shown in Figure 1 (C, F). For the GE/GA MRP-DHA NMs, particle sizes larger than 1000 nm are not shown in Figure 1 (C, F). As illustrated in Figure 1 (C, F), as the core-wall ratio decreased, the SC/GA MRP-DHA NMs exhibited a decrease in particle size; whereas the

SPI/GA MRP-DHA NMs displayed the smallest particle size at 1:3. Furthermore, the PDI of the GE/GA MRP-DHA NMs tended to first decrease, then increase, and decrease again. Reducing the core-wall ratio from 1:2 to 1:5 effectively increased the PDI of the SC/GA MRP-DHA NMs and SPI/GA MRP-DHA NMs. This implies that interactions between the complex and the emulsion resulted in emulsion polymerization due to lowering the core-wall ratio and increasing the concentration of the wall material. A core-wall ratio of 1:2 produced the lowest PDI values of 0.206, 0.233, and 0.391. The ideal core-wall ratio was therefore determined to be 1:2.

### 3.2. Storage stability of MRP-DHA NMs

The effect of storage time on the particle size and PDI of SC/GA MRP-DHA NMs, SPI/GA MRP-DHA NMs and GE/GA MRP-DHA NMs is illustrated in Figure 2 (A, B). As depicted in Figure 2 (A, B), the particle size and PDI of SC/GA MRP-DHA NMs increased from 239 nm and 0.23 to 589 nm and 0.51 after a month of room temperature storage due to the extended storage period. The particle size and

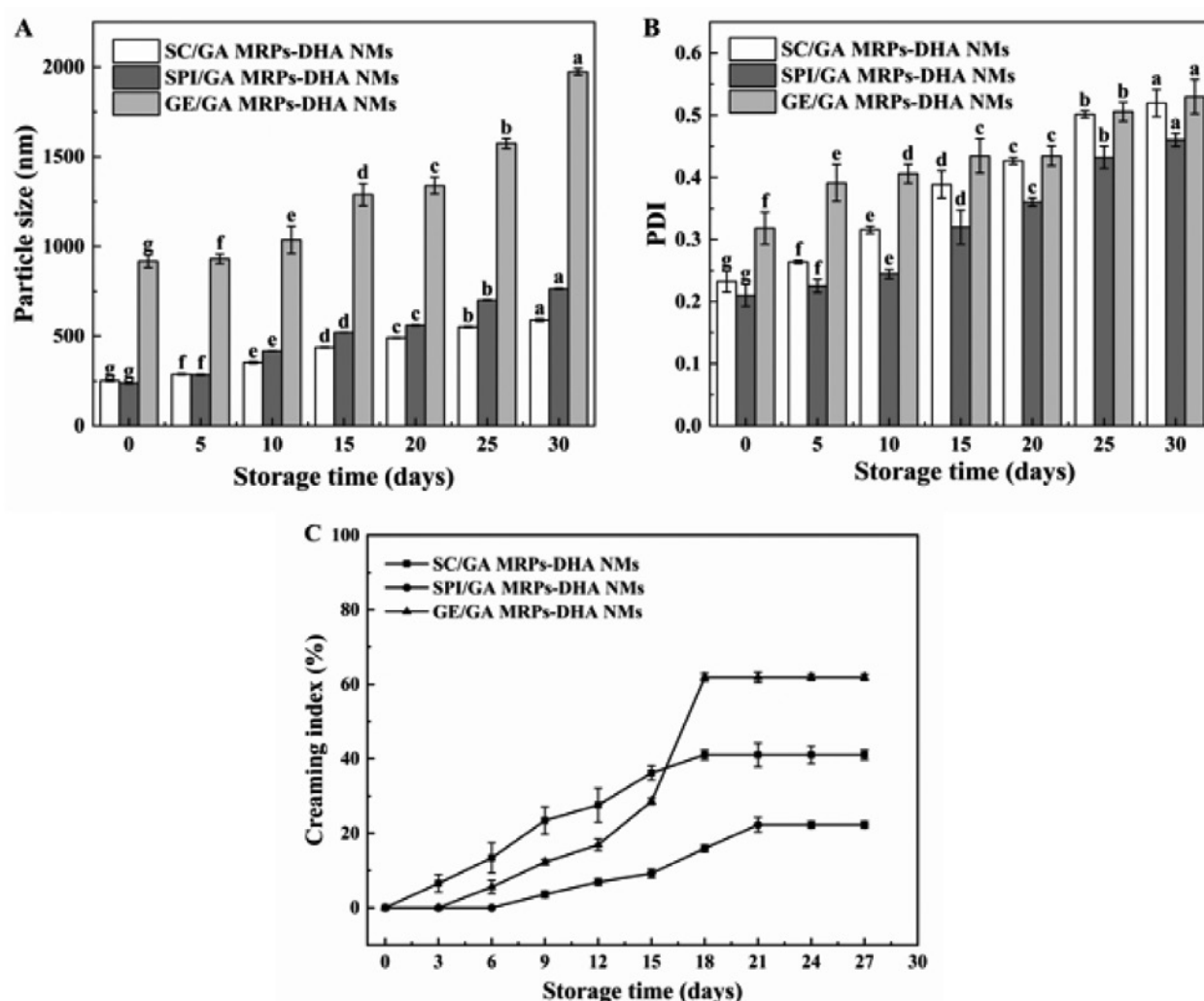


**FIGURE 2.** Effect of storage time on particle size (A), PDI (B) and creaming index (C) of the MRPs-DHA NMs. All three MRPs-DHA NMs were prepared under optimal preparation conditions (total mass concentration 5%, ultrasonic time 20 minutes, core-wall ratio 1:2). The results are expressed as mean  $\pm$  standard deviation ( $n = 3$ ). In Figures A and B, significance analysis was conducted on the changes in particle size and PDI of the same sample over storage time. For the same sample at different time points, different superscripts indicate significant differences ( $p < 0.05$ ), as determined by Fisher's least significant difference (LSD) test within the analysis of variance (ANOVA).

PDI of the SPI/GA MRPs-DHA NMs also increased from 252 nm and 0.21 to 764 nm and 0.46, respectively. Additionally, the particle size and PDI of the GE/GA MRPs-DHA NMs significantly increased to 1973 nm and 0.63, in comparison to those of the former two emulsions.

The CI of the SC/GA MRPs-DHA NMs, SPI/GA MRPs-DHA NMs and GE/GA MRPs-DHA NMs after 27 days of storage at room temperature is depicted in Figure 2C. The CI is used to measure emulsion stability, with a lower CI indicating greater stability. After one week of storage, the SC/GA MRPs-DHA NMs, SPI/GA MRPs-DHA NMs and GE/GA MRPs-DHA NMs exhibited relatively low

CI, as shown in Figure 4B. This improved emulsion stability can be attributed to the protein-polysaccharide complexes formed through the Maillard reaction, which successfully maintained the oil-in-water (O/W) emulsions even under harsh conditions such as high ionic strength, low pH, and heat treatment, thereby enhancing spatial stability (Nicoletti, 2019). However, the CI for each of the three emulsions increased progressively during the storage period. The depletion flocculation mechanism caused by a high concentration of non-adsorbed GA can lead to emulsion instability, and an increase in CI. Additionally, GE/GA MRPs-DHA NMs demonstrate a relatively high CI, indicating that dominant van der

Waals-London attractive forces may contribute to flocculation during the encapsulation of oil droplets within electron-neutral coacervates.

Taking into account the changes in emulsion particle size, PDI, and CI during storage, SPI/GA MRPs-DHA NM showed the best emulsion stability. This is due to the excellent emulsifying and amphiphilic properties of SPI, which reduce the surface tension at the oil-water interface and create a stable emulsion system. Moreover, the emulsifying activity of SPI was improved by the Maillard reaction between SPI and GA, resulting in enhanced emulsifying stability in the SPI/GA MRPs as the polysaccharide chain molecular weight increased (Wang *et al.*, 2018). Chu *et al.* (2023) also reported that Maillard reaction with oat  $\beta$ -glucan changed the structure of SPI, further leading to the enhancement of its functional properties.

### 3.3. Physical and chemical properties of different MRPs-DHA NPs

Table 1 indicates that the moisture content of SPI/GE MRPs-DHA NPs was lower compared to SC and GE/GA MRPs-DHA NPs. The stability of NP powder storage is influenced by its moisture content. SPI/GE MRPs-DHA NPs with lower moisture contents can effectively impede microbiological and metabolic activities in food systems, thus preventing oxidation and spoilage to ensure product stability. Solubility is a crucial factor affecting the quality of DHA NP powder. Its superior solubility is necessary for both direct consumption as a reconstituted drink and manufacturing for use as a nutritional addition

TABLE 1. The moisture content, solubility, and wettability of the MRPs-DHA NPs.

Sample	Moisture content (%)	Solubility (%)	Wettability (s)
SC/GA MRPs-DHA NPs	1.58±0.15 <sup>b</sup>	95.79±0.55 <sup>b</sup>	208±3 <sup>b</sup>
SPI/GA MRPs-DHA NPs	1.53±0.07 <sup>b</sup>	97.05±0.48 <sup>a</sup>	183±5 <sup>c</sup>
GE/GA MRPs-DHA NPs	2.40±0.10 <sup>a</sup>	91.41±0.53 <sup>c</sup>	381±11 <sup>a</sup>

All three MRPs-DHA NPs were prepared under optimal preparation conditions (total mass concentration 5%, ultrasonic time 20 minutes, core-wall ratio 1:2). The values are the mean ± standard deviations (n = 3). Different superscripts in the same column represent significant differences ( $p < 0.05$ ), as determined by Fisher's least significant difference (LSD) test within the analysis of variance (ANOVA).

to other foods. Table 1 shows significant differences ( $p < 0.05$ ) in the solubilities of SC/GA MRPs-DHA NPs, SPI/GA MRPs-DHA NPs and GE/GA MRPs-DHA NPs, which are 95.79%, 97.05%, and 91.41%, respectively. The presence of carriers and hydrophilic groups in the substrate structure significantly impacts solubility. The consumption of SPI amino groups during the Maillard reaction with GA, as well as the introduction of polysaccharide chains with numerous hydroxyl groups, considerably enhance the solubility of the SPI/GA MRPs-DHA NPs. Good water dispersibility is an essential quality for using DHA powder in food fortifications. The wetting times obtained through experimentation varied significantly ( $p < 0.05$ ), ranging from 183 s for SPI/GA MRPs-DHA to 381 s for GE/GA MRPs-DHA. Interactions between peptide bonds or side chains of amino acids in SPI and water molecules improve the wettability of SPI/GA MRPs-DHA NPs by facilitating water molecules to adhere to the particle surface.

### 3.4. EE and LC of MRPs-DHA NPs

The impacts of core-wall ratio on encapsulation efficiency and loading capacity of the MRPs-DHA NPs are shown in Figure 3. Results in Figure 6 indicate that lowering the core-wall ratio for SC/GA MRPs-DHA NPs, SPI/GA MRPs-DHA NPs and GE/GA MRPs-DHA NPs leads to reduced LC but increased EE. Specifically, at a core-wall ratio of 1:2, the encapsulation efficiencies of SC/GA MRPs-DHA

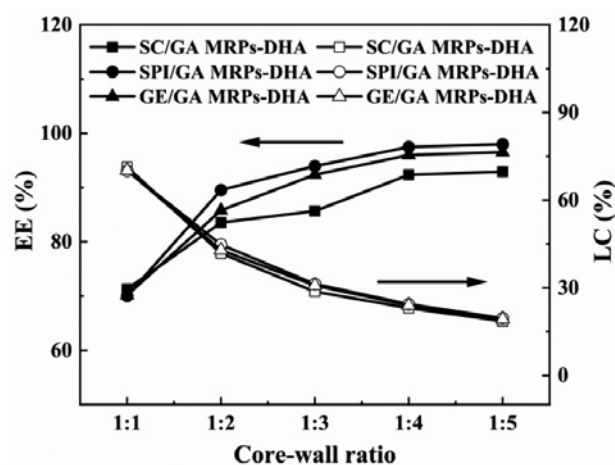


FIGURE 3. Effect of core-wall ratio on encapsulation efficiency and loading capacity of the MRPs-DHA NPs. All three MRPs-DHA NPs were prepared under optimal preparation conditions (total mass concentration 5%, ultrasonic time 20 minutes, core-wall ratio 1:2). The results are expressed as mean ± standard deviation (n = 3).

NPs, SPI/GA MRPs-DHA NPs and GE/GA MRPs-DHA NPs were 83.57%, 89.57%, and 85.82%, respectively. The loading capacities at the same core-wall ratio were 41.78%, 44.79%, and 42.91%, respectively. Comparison with reported values for nanoencapsulated EPA/DHA with the sodium caseinate-gum arabic complex, which exhibited an encapsulation efficiency of 78.88% and a loading capacity of 32.66% (Ilyasoglu and El, 2014), suggested that the protein-polysaccharide MRPs in this study positively impact the encapsulation efficiency and loading capacity of DHA.

Furthermore, the data in Figure 3 demonstrate that the loading capacities of SC/GA MRPs-DHA NPs, SPI/GA MRPs-DHA NPs and GE/GA MRPs-DHA NPs are comparable and decrease as the core wall ratio decreases. A core-wall ratio of 1:2 was chosen as the ideal ratio for manufacturing DHA NPs because it allows for less wall material to be used while still ensuring effective encapsulation. This option has financial benefits in addition to energy savings. The higher EE and LC of SPI/GA MRPs-DHA NPs can minimize wall material reduction, reduce product volume and weight, and effectively control the antioxidant properties of the product.

### 3.5. Morphology of MRPs-DHA NPs

The micro-morphology of the nanocapsules was characterized by OM, SEM, and TEM (Figure 4A, B and C). OM images of SC/GA MRPs-DHA NMs, SPI/GA MRPs-DHA NMs and GE/GA MRPs-DHA NMs showed no significant differences, and representative images of SPI/GA MRPs-DHA NMs are depicted in Figure 4A. The SEM image of the GE/GA MRPs-DHA NPs are shown in Figure 4B because the particle sizes of the SC/GA MRPs-DHA NPs and SPI/GA MRPs-DHA NPs may be too small to be sufficiently scanned by SEM. According to the TEM images of SC/GA MRPs-DHA NMs and SPI/GA MRPs-DHA NMs, there are no notable variations in structure. Therefore, the SPI/GA MRPs-DHA NMs are used as the representative sample in Figure 4C.

The MRPs-DHA NMs exhibited uniformly sized and evenly dispersed circular oil droplets, as seen in the OM image (Figure 4A) at 4000x magnification. It was clear from the SEM and TEM images (Figure 4B and C) that MRPs-DHA had a typical spherical structure and smooth surface. Additionally, the absence of apparent cracks or fissures on the particle surface ensures low permeability of the NPs, enhanc-

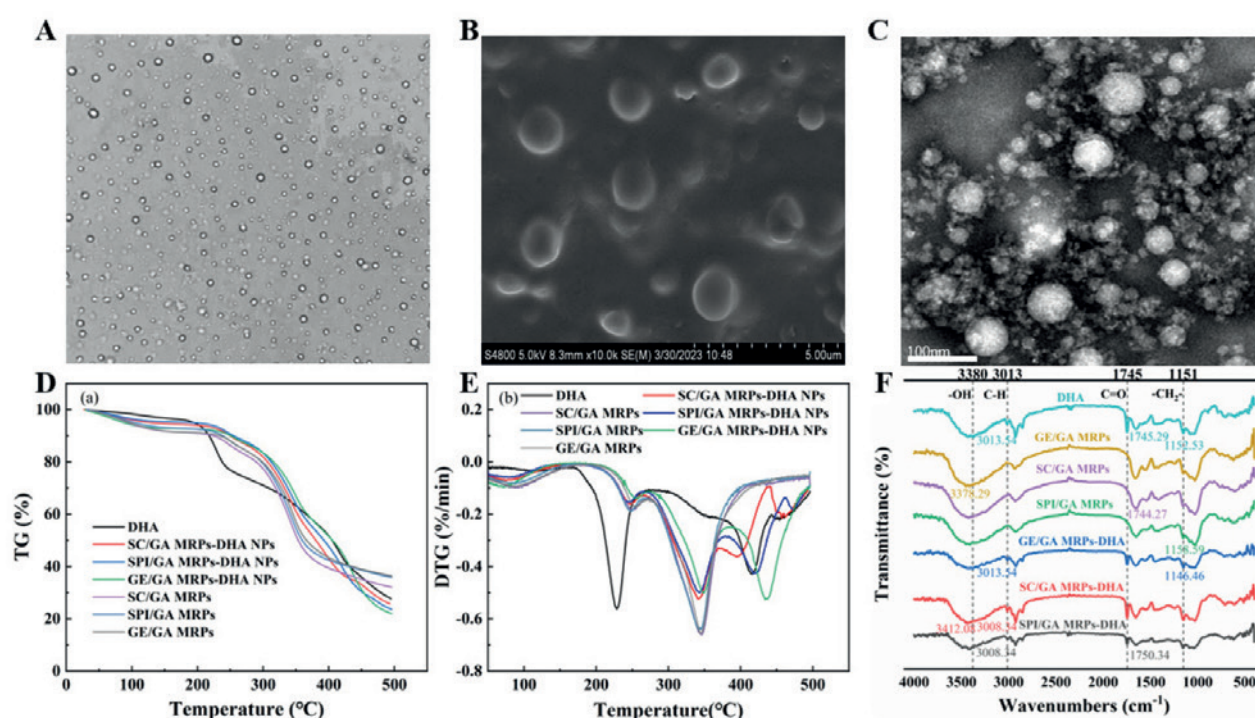


FIGURE 4. Characterization of MRPs-DHA NPs (A) OM image, (B) SEM image, (C) TEM image, (D) TG curves, (E) DTG curves, (F) FTIR spectra. All three MRPs-DHA NPs were prepared under optimal preparation conditions (total mass concentration 5 %, ultrasonic time 20 minutes, core-wall ratio 1:2).

ing DHA protection. Moreover, a few tiny pores are observed on SEM image, likely resulting from the contraction of liquid particles during the freeze-drying process (Wang and Sun, 2021). Similar porous microcapsule morphologies have been reported in a study involving stearidonic acid soybean oil with modified gelatin-gum arabic Maillard coacervates as the wall material (Ifeduba and Akoh, 2016). These findings show that the protein-polysaccharide Maillard wall material positively impacts the encapsulation efficiency of DHA, which forms a smooth, dense layer that prevents DHA oxidation and reduces oil leakage.

### 3.6. TGA

The TG/DTG curves for DHA, shown in Figure 4 (D, E), indicate that the decomposition process of DHA oil commences at temperatures exceeding 200 °C. The highest rates of decomposition are found in the temperature range of 228 °C to 418 °C. The first slight weight loss (between 30 and 100 °C) of MRPs-DHA NPs corresponded to the loss of free water (Saldo *et al.*, 2002). The TG/DTG curves for the MRPs DHA NPs exhibited significant weight loss in the temperature range of 200-360 °C. This could result from the mass loss caused by the evaporation of DHA oil and the decomposition of Maillard wall material (Xiao *et al.*, 2020). The mass loss of the three NP samples was 25.16%, 22.75%, and 23.87%, respectively. At temperatures above 360 °C, the weight loss of the NPs likely results from the extensive decomposition of internal DHA and the residual wall materials (Xiao *et al.*, 2015). Additionally, the temperature at which DHA exhibited its maximum weight loss rate shifted from 228 °C to 350 °C, which proved the effectiveness of nano-encapsulation of DHA by MRPs. Furthermore, SPI/GA MRPs-DHA NPs have the lowest weight loss, which shows the best thermal stability.

### 3.7. FTIR spectroscopy

The assignments of FTIR spectral features were completed by comparing them with the literature data and are presented in Figure 4E. The stretching vibration of -OH is correlated with the absorption peak at 3380  $\text{cm}^{-1}$ , suggesting the presence of water or initial oxidation products in the oil (Zhang

*et al.*, 2012). The C-H vibrational band of hydrocarbon long-chain polyunsaturated fatty acids may be responsible for the band at wavenumber 3013  $\text{cm}^{-1}$ . The ester bond is linked to the distinctive peak at 1745.29  $\text{cm}^{-1}$ , which is attributed to the absorption of DHA. Additionally, characteristic absorption peaks appeared at 1151  $\text{cm}^{-1}$  related to -CH<sub>2</sub>-. Moreover, the band observed at 1404-1419  $\text{cm}^{-1}$  is associated with O-H bending, while the presence of bound water in the wall materials is reflected by the peak at 1641  $\text{cm}^{-1}$ . Furthermore, the bands corresponding to hydrogen bonding shifted from 3380  $\text{cm}^{-1}$  to 3412  $\text{cm}^{-1}$ , suggesting the formation of strong hydrogen bonds between the MRPs and DHA. Similar FTIR patterns were reported by Wang *et al.* (2020) for the encapsulation of algal oil with octenyl-succinic anhydride (OSA), inulin (IN), and maltodextrin (MD). The researchers noted that the FTIR peaks of the OSA/MD/IN particles emerged at 3386  $\text{cm}^{-1}$  for OH stretching vibration, 3014  $\text{cm}^{-1}$  for C-H stretching, 1745  $\text{cm}^{-1}$  for C=O stretching, and 1153  $\text{cm}^{-1}$  for C-O-C stretching. Additionally, the hydroxyl group stretching vibration peak of the OSA/MD/IN NPs shifted from 3405  $\text{cm}^{-1}$  to 3386  $\text{cm}^{-1}$ .

FTIR analysis revealed characteristic peaks for pure DHA at wavenumbers 1151, 1745, 3013, and 3080  $\text{cm}^{-1}$ . Similar absorption peaks are observed for SC/GA MRPs-DHA NPs, SPI/GA MRPs-DHA NPs and GE/GA MRPs-DHA NPs at these specific bands, and the characteristic peaks were significantly weakened, indicating that the encapsulation process does not change the original properties of DHA, and the interaction between DHA and MRPs wall materials changed the microenvironment and prevented functional groups from vibrating too much (Martins *et al.*, 2020). Wang *et al.* (2011) encapsulated garlic oil with  $\beta$ -cyclodextrin, and the characteristic absorption peak of garlic oil almost completely disappeared in the atlas of embedded matter. FTIR analysis also confirmed the effectiveness of the SC/GA MRPs, SPI/GA MRPs and GE/GA MRPs wall materials for DHA nano-encapsulation.

### 3.8. Storage stability of MRPs-DHA NPs

POV changes were measured to evaluate the stability of nano-capsules containing different wall materials. As shown in Figure 5, the POV of unencapsulated DHA rapidly accelerated with increasing storage

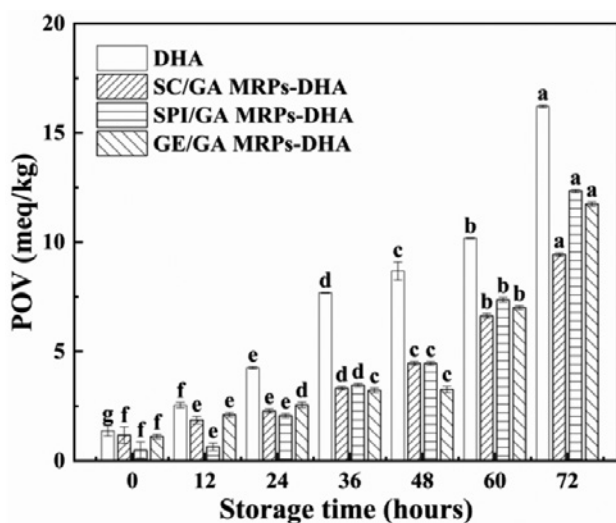


**FIGURE 5.** POV of DHA, SC/GA MRPs-DHA NPs, SPI/GA MRPs-DHA NPs and GE/GA MRPs-DHA NPs during storage time. All three MRPs-DHA NPs were prepared under optimal preparation conditions (total mass concentration 5 %, ultrasonic time 20 minutes, core-wall ratio 1:2). The results are expressed as mean  $\pm$  standard deviation ( $n = 3$ ). Different lowercase letters indicate significant differences ( $p < 0.05$ ), as determined by Fisher's least significant difference (LSD) test within the analysis of variance (ANOVA).

time, close to the threshold value of 10.24 meq/kg as specified in the GB 15196-2015, Edible Oil and Fat Products, the Chinese National Standard for Food Safety after 48 hours. Conversely, MRPs-DHA NPs had a slower increase in POV, confirming that the nano-capsule products exhibited efficient heat-resistance performance and helped protect DHA oil quality. Chen *et al.* (2016) reported that the POV of DHA-rich oil reached a maximum level of 52.27 meq  $O_2$ /kg and 459.93 meq  $O_2$ /kg at 4 °C and 45 °C during eight weeks of storage. Seyed *et al.* (Ojagh and Hasani, 2018) also reported that nano-encapsulated fish oil showed better oxidative stability against lipid oxidation in comparison with unencapsulated fish oil.

#### 4. CONCLUSIONS

In this study, the physicochemical characterization of DHA NMs prepared from three different Maillard wall materials, and DHA NPs prepared by freeze-drying was investigated. Among the three nano-systems, SPI/GA MRPs-DHA exhibited the highest EE and LC, the lowest moisture content, superior solubility and wettability, minimal changes in CI, particle size, and PDI during storage, and a lower POV, which provided optimal protection for

DHA oil during storage. TGA demonstrated that SPI/GA MRPs-DHA NPs showed the least mass loss during the programmed warming process. Additionally, the temperature corresponding to the maximum weight loss of DHA oil shifted from 228 to 350 °C, which indicates its excellent thermal stability.

It can be concluded that SPI/GA MRPs are the optimal wall materials, as they can enhance the encapsulation efficiency (EE), loading capacity (LC), and physicochemical stability of DHA. In contrast, SC/GA MRPs and GE/GA MRPs exhibit certain deficiencies, particularly GE/GA MRPs, which have larger particle sizes and lower EE, among other issues. SPI/GA MRPs are promising and could be employed for nano-encapsulation of most oil-soluble bioactive ingredients.

#### RESEARCH DATA POLICY DATA AVAILABILITY

The data underlying this article will be shared on reasonable request to the corresponding author.

#### ACKNOWLEDGMENTS

Not applicable.

#### DECLARATION OF COMPETING INTEREST

The authors of this article declare that they have no financial, professional or personal conflicts of interest that could have inappropriately influenced this work.

#### FUNDING SOURCES

This work was supported by Science and Technology Research projects of Shijiazhuang City (No.231170092A).

#### AUTHORSHIP CONTRIBUTION STATEMENT

L. Zhou: Conceptualization, Investigation, Formal analysis, Writing – original draft, Writing – review & editing. S. Yuan: Conceptualization, Investigation. T. Chang: Investigation. T. Li: Investigation. J. Hao: Conceptualization, Resources, Supervision. J. Liu: Conceptualization, Writing – review & editing, Supervision, Project administration, Funding acquisition.

**Abbreviations:**

CI	Creaming Index
DHA	Docosahexaenoic Acid
EE	Encapsulation Efficiency
FTIR	Fourier Transform Infrared
GA	Gum Arabic
GE	Gelatine
LC	Loading Capacity
MRPs	Maillard Reaction Products
NMs	Nanoemulsions
NPs	Nanoparticles
OM	Optical Microscopy
SC	Sodium Caseinate
SEM	Scanning Electron Microscope
SPI	Soy Protein Isolate
TEM	Transmission Electron Microscopy
TGA	Thermogravimetric Analysis

**REFERENCES**

- Anal AK, Shrestha S and Sadiq MB. 2019. Biopolymeric-based emulsions and their effects during processing, digestibility and bioaccessibility of bioactive compounds in food systems. *Food Hydrocolloids*. **87**, 691-702. <https://doi.org/10.1016/j.foodhyd.2018.09.008>
- Awuchi CG, Morya S, Dendegh TA, Okpala COR, Korzeniowska M. 2022. Nanoencapsulation of food bioactive constituents and its associated processes: A revisit. *Bioresour. Technol. Rep.* **19**, 101088. <https://doi.org/10.1016/j.biteb.2022.101088>
- Botrel DA, de Barros Fernandes RV, Borges SV, Yoshida MI. 2014. Influence of wall matrix systems on the properties of spray-dried microparticles containing fish oil. *Food Res. Int.* **62**, 344-352. <https://doi.org/10.1016/j.foodres.2014.02.003>
- Chen W, Wang H, Zhang K, Gao F, Chen S, Li D. 2016. Physicochemical Properties and Storage Stability of Microencapsulated DHA-Rich Oil with Different Wall Materials. *Appl. Biochem. Biotechnol.* **179**, 1129-1142. <http://dx.doi.org/10.1007/s12010-016-2054-3>
- Chu Zn, Zhang Qy, Li Xh, Xue B, Sun T, Xie J. 2023. Effect of Oat  $\beta$ -Glucan on the Structure and Properties of Soybean Protein Isolate During Maillard Reaction. *Plant Foods Hum. Nutr.* **78**, 552-556. <http://dx.doi.org/10.1007/S11130-023-01092-4>
- Dey TK, Koley H, Ghosh M, Dey S, Dhar P. 2019. Effects of nano-sizing on lipid bioaccessibility and ex vivo bioavailability from EPA-DHA rich oil in water nanoemulsion. *Food Chem.* **275**, 135-142. <https://doi.org/10.1016/j.foodchem.2018.09.084>
- García E, Gutiérrez S, Nolasco H, Carreón L, Arjona O. 2005. Lipid composition of shark liver oil: effects of emulsifying and microencapsulation processes. *Eur. Food Res. Technol.* **222**, 697-701. <http://dx.doi.org/10.1007/s00217-005-0129-4>
- Ghasemi S, Jafari SM, Assadpour E, Khomeiri M. 2017. Production of pectin-whey protein nano-complexes as carriers of orange peel oil. *Carbohydr. Polym.* **177**, 369-377. <https://doi.org/10.1016/j.carbpol.2017.09.009>
- Ghasemi S, Jafari SM, Assadpour E, Khomeiri M. 2018. Nanoencapsulation of d-limonene within nanocarriers produced by pectin-whey protein complexes. *Food Hydrocolloids*. **77**, 152-162. <https://doi.org/10.1016/j.foodhyd.2017.09.030>
- Hosseini A, Jafari SM, Mirzaei H, Asghari A, Akhavan S. 2015. Application of image processing to assess emulsion stability and emulsification properties of Arabic gum. *Carbohydr. Polym.* **126**, 1-8. <http://dx.doi.org/10.1016/j.carbpol.2015.03.020>
- Ifeduba EA, Akoh CC. 2016. Microencapsulation of stearidonic acid soybean oil in Maillard reaction-modified complex coacervates. *Food Chem.* **199**, 524-532. <https://doi.org/10.1016/j.foodchem.2015.12.011>
- Ilyasoglu H, El SN. 2014. Nanoencapsulation of EPA/DHA with sodium caseinate-gum arabic complex and its usage in the enrichment of fruit juice. *LWT - Food Sci. Technol.* **56**, 461-468. <https://doi.org/10.1016/j.lwt.2013.12.002>
- Jafari SM, Assadpour E, He Y, Bhandari B. 2008. Encapsulation Efficiency of Food Flavours and Oils during Spray Drying. *Drying Technol.* **26**, 816-835. <http://dx.doi.org/10.1080/07373930802135972>
- Li J, Hou X, Jiang L, Xia D, Anjun Chen A, Li S, Li Q, Gu X, Mo X, Zhang Z. 2022. Optimization and characterization of Sichuan pepper (*Zanthoxylum bungeanum* Maxim) resin microcapsule encapsulated with  $\beta$ -cyclodextrin. *LWT--Food Sci. Technol.* **171**, 114120. <https://doi.org/10.1016/j.lwt.2022.114120>
- Liu M, Yang C, Liu E, Zhang F, Meng X, Liu B. 2021. Effect of environmental stresses on

- physicochemical properties of ALA oil-in-water nanoemulsion system prepared by emulsion phase inversion. *Food Chem.* **343**, 128475. <https://doi.org/10.1016/j.foodchem.2020.128475>
- Liu Xy, Zhang Xy, Ding Lx, Jin H, Chen N, Huang X, Jin Y, Cai Z. 2023. Natural egg yolk emulsion as wall material to encapsulate DHA by two-stage homogenization: Emulsion stability, rheology analysis and powder properties. *Food Res. Int.* **167**, 112658. <https://doi.org/10.1016/j.foodres.2023.112658>
- Lv W and Xu D. 2022. Docosahexaenoic Acid Delivery Systems, Bioavailability, Functionality, and Applications: A Review. *Foods*. **11**, 2685-2685. <http://dx.doi.org/10.3390/FOODS11172685>
- Martins LNSB, Venceslau AdFA, Carvalho LB, Jaime C, Cardoso MG, Pinto LMA. 2020. Inclusion complex of Callistemon viminalis essential oil prepared by kneading. *J. Inclusion Phenom. Macrocyclic Chem.* **97**, 109-119. <http://dx.doi.org/10.1007/s10847-020-00989-w>
- Moghadam FV, Pourahmad R, Mortazavi A, Davoodi D, Azizinezhad R. 2019. Use of Fish Oil Nanoencapsulated with Gum Arabic Carrier in Low Fat Probiotic Fermented Milk. *Food Sci Anim Resour.* **39**, 309-323. <http://dx.doi.org/10.5851/kosfa.2019.e25>
- Mudalige T, Qu H, Van Haute D, Ansar SM, Paredes A, Ingle T. 2019. Chapter 11 - Characterization of Nanomaterials: Tools and Challenges, In López Rubio A (Ed.) *Nanomaterials for Food Applications*. Elsevier, Jefferson, 313-353. <https://doi.org/10.1016/B978-0-12-814130-4.00011-7>
- Nicoletti VR. 2019. O/W Emulsions Stabilized by Interactions Between Proteins and Polysaccharides, In Vânia Regina Nicoletti Telis (Ed.) *Encyclopedia of Food Chemistry*. São Paulo State University – Unesp, Brazil, 494-498. <https://doi.org/10.1016/B978-0-08-100596-5.21483-2>
- Ojagh SM and Hasani S. 2018. Characteristics and oxidative stability of fish oil nano-liposomes and its application in functional bread. *J. Food Meas. Charact.* **12**, 1084-1092. <http://dx.doi.org/10.1007/s11694-018-9724-5>.
- Pirestani S, Nasirpour A, Keramat J, Desobry S, Jasniewski J. 2018. Structural properties of canola protein isolate-gum Arabic Maillard conjugate in an aqueous model system. *Food Hydrocolloids.* **79**, 228-234. <https://doi.org/10.1016/j.foodhyd.2018.01.001>
- Saldo J, Sendra E, Guamis B. 2002. Changes in water binding in high-pressure treated cheese, measured by TGA (thermogravimetric analysis). *Innovative Food Sci. Emerging Technol.* **3**, 203-207. [https://doi.org/10.1016/S1466-8564\(02\)00047-4](https://doi.org/10.1016/S1466-8564(02)00047-4)
- Su Z, Han C, Liu E, Zang F, Liu B, Meng X. 2021. Formation, characterization and application of arginine-modified chitosan/gamma-poly glutamic acid nanoparticles as carrier for curcumin. *Int. J. Biol. Macromol.* **168**, 215-222. <https://doi.org/10.1016/j.ijbiomac.2020.12.050>
- Wang J, Cao Y, Sun B, Wang C. 2011. Physicochemical and release characterisation of garlic oil- $\beta$ -cyclodextrin inclusion complexes. *Food Chem.* **127**, 1680-1685. <https://doi.org/10.1016/j.foodchem.2011.02.036>
- Wang LH, Sun X, Huang GQ, Xiao JX. 2018. Conjugation of soybean protein isolate with xylose/fructose through wet-heating Maillard reaction. *J. Food Meas. Charact.* **12**, 2718-2724. <http://dx.doi.org/10.1007/s11694-018-9889-y>
- Wang Y and Sun S. 2021. Multiscale pore structure characterization based on SEM images. *Fuel.* **289**, 119915. <https://doi.org/10.1016/j.fuel.2020.119915>
- Wang Y, Zheng Z, Wang K, Tang C, Liu Y, Li J. 2020. Prebiotic carbohydrates: Effect on physicochemical stability and solubility of algal oil nanoparticles. *Carbohydr. Polym.* **228**, 115372. <https://doi.org/10.1016/j.carbpol.2019.115372>
- Xiao Q, Chen G, Zhang Y, Weng H, Cai M, Xiao A. 2020. Evaluation of a novel self-emulsifiable dodecanyl succinylated agarose in microencapsulation of docosahexaenoic acid (DHA) through spray-chilling process. *Int. J. Biol. Macromol.* **163**, 2314-2324. <https://doi.org/10.1016/j.ijbiomac.2020.09.108>
- Xiao Z, Li W and Zhu G. 2015. Effect of wall materials and core oil on the formation and properties of styralyl acetate microcapsules prepared by complex coacervation. *Colloid Polym. Sci.* **293**, 1339-1348. <http://dx.doi.org/10.1007/s00396-015-3515-x>
- Zhang Q, Liu C, Sun Z, Hu X, Shen Q, Wu J. 2012. Authentication of edible vegetable oils adulterated with used frying oil by Fourier Transform Infrared Spectroscopy. *Food Chem.* **132**, 1607-1613. <https://doi.org/10.1016/j.foodchem.2011.11.129>